Development 136, 373-382 (2009) doi:10.1242/dev.030858

RIM-BP3 is a manchette-associated protein essential for spermiogenesis

Jing Zhou[1,*], Ya-Rui Du[1,*], Wei-Hua Qin[1,†], Ye-Guang Hu[1], Yan-Nv Huang[1], Lan Bao[2], Daishu Han[3], Ahmed Mansouri[4] and Guo-Liang Xu[1,‡]

During spermiogenesis, round spermatids are converted into motile sperm in mammals. The mechanisms responsible for sperm morphogenesis are poorly understood. We have characterized a novel protein, RIM-BP3, with a specialized function in spermatid development in mice. The RIM-BP3 protein is associated with the manchette, a transient microtubular structure believed to be important for morphogenesis during spermiogenesis. Targeted deletion of the *RIM-BP3* gene resulted in male infertility owing to abnormal sperm heads, which are characterized by a deformed nucleus and a detached acrosome. Consistent with its role in morphogenesis, the RIM-BP3 protein physically associates with Hook1, a known manchette-bound protein required for sperm head morphogenesis. Interestingly, RIM-BP3 does not interact with the truncated Hook1 protein characterized in *azh* (*abnormal spermatozoon head*) mutant mice. Moreover, *RIM-BP3* and *Hook1* mutant mice display several common abnormalities, in particular with regard to the ectopic positioning of the manchette within the spermatid, a presumed cause of sperm head deformities. These observations suggest an essential role for RIM-BP3 in manchette development and function through its interaction with Hook1. As the occurrence of deformed spermatids is one of the common abnormalities leading to malfunctional sperm, identification of RIM-BP3 might provide insight into the molecular cue underlying causes of male infertility in humans.

KEY WORDS: *RIM-BP3* (*Rimbp3*), *Hook1*, Spermatid manchette, Spermiogenesis, Mouse

INTRODUCTION

Mammalian male fertility depends on the successful generation of motile sperm that carry an intact paternal genome and are capable of fertilizing the egg. Spermatogenesis is a complex and tightly regulated process that can be divided into three phases: mitosis (self-renewal and multiplication of spermatogonia), meiosis (reduction of the chromosomal number from diploid to haploid), and spermiogenesis (differentiation of haploid spermatids into sperm). During spermiogenesis, haploid germ cells undergo dramatic morphological changes, eventually forming functional sperm. These changes include elongation and condensation of the nucleus, formation of the acrosome and flagella, and disposal of unnecessary cytoplasm. A unique microtubular structure, termed manchette, appears transiently in the developing spermatid. The manchette surrounds the nucleus and is believed to assist in both the nuclear shaping and in the intramanchette transport of proteins (Kierszenbaum et al., 2007).

Spermatid development requires the function of genes expressed under stringent temporal and spatial regulation. Using gene targeting technology, around 20 male germ cell-specific genes have been identified to play important roles during spermiogenesis (Matzuk and Lamb, 2002). These genes are involved in the regulation of acrosome biogenesis (*Hrb*, *Gopc* and *Csnk2a2*) (Escalier et al., 2003; Kang-Decker et al., 2001; Yao et al., 2002), tail formation (*Tektin-t*, *Vdac3*, *Sepp1*, *Akap4* and *Spag6*) (Olson et al., 2005; Sampson et al., 2001; Sapiro et al., 2002; Shirohzu et al., 2002; Tanaka et al., 2004) and chromosomal packaging (*Prm1*, *Prm2*, *Tnp1*, *Tnp2* and *H1t2*) (Fuhrmann et al., 2001; Martianov et al., 2005; Tanaka et al., 2005; Yu et al., 2000), among others. Despite the identification of genes involved in various aspects of spermiogenesis, the mechanism of nuclear shaping is still poorly understood.

The manchette as a transient microtubular structure assembles concurrently with the elongation and condensation of spermatid nucleus and growth of the centrosome-derived axoneme (Kierszenbaum, 2002). It has been proposed that the microtubular manchette, which could provide a track for vesicles to mobilize, contributes to the transport of molecules to spermatid tail and facilitates nucleocytoplasmic transport across the relocated nuclear pore complexes (Kierszenbaum and Tres, 2004). Vesicles might remain linked to the microtubules in a 'holding pattern' until microtubule-based motors recruit them for transport. A candidate vesicle-microtubule adaptor is Hook1, a manchette-associated protein that is truncated in the *azh* mutant mouse, which is characterized by abnormal sperm heads (Mendoza-Lujambio et al., 2002). Murine Hook1 belongs to the Hook protein family, which is conserved from fly to mammals (Kramer and Phistry, 1999). Previous work in *Drosophila* suggests that the Hook protein plays a role in the endocytosis of transmembrane ligands or their transport to multivesicular bodies (Kramer and Phistry, 1996; Kramer and Phistry, 1999). Murine Hook1 is located in the manchette of developing spermatids (Mendoza-Lujambio et al., 2002). The loss of Hook1 function results in ectopic positioning of microtubular structures within the spermatid (Mendoza-Lujambio et al., 2002), causing the mouse *azh* phenotype, which is characterized by abnormal head shape (Cole et al., 1988), head dislocation and spermatid tail coiling

[1]The State Key Laboratory of Molecular Biology, [2]The Key Laboratory of Cell Biology, Institute of Biochemistry and Cell Biology, Shanghai Institutes for Biological Sciences, Chinese Academy of Sciences, 320 Yueyang Road, Shanghai 200031, China. [3]Department of Cell Biology, Institute of Basic Medical Sciences, Chinese Academy of Medical Sciences, 5 Dong Dan San Tiao, Beijing 100005, China. [4]Max Planck Institute of Biophysical Chemistry, Department of Molecular Cell Biology, Am Fassberg, 37077 Goettingen, Germany.

*These authors contributed equally to this work
†Present address: Ludwig Maximilians University Munich, Department of Biology II, 82152 Martinsried, Germany
‡Author for correspondence (e-mail: glxu@sibs.ac.cn)

Accepted 19 November 2008

(Mochida et al., 1999). Based on these studies, Hook1 was proposed to be essential for the manchette development and function.

We have characterized RIM-BP3 (Rimbp3 – Mouse Genome Informatics), a novel manchette-associated protein. It belongs to the RIM-binding protein (RIM-BP) family (Mittelstaedt and Schoch, 2007). RIM-BPs have been proposed to function as adaptors in the process of vesicle fusion and release (Hibino et al., 2002). RIM-BP1 and RIM-BP2 were identified as binding partners of the presynaptic active zone proteins RIM1 and RIM2 as well as for voltage-gated Ca^{2+}-channels (Wang et al., 2000; Hibino et al., 2002). All three RIM-BP members are large multidomain proteins containing three SH3-domains, two or three contiguous fibronectin type III domains, and paralog-specific regions at the N terminus and between the clustered domains (Mittelstaedt and Schoch, 2007). These signature domains and known interactions with Ca^{2+}-channels and RIM proteins suggest that RIM-BPs provide a scaffold for other regulatory proteins. The RIM-BP proteins are particularly conserved in invertebrates and vertebrates throughout the SH3- and FNIII domains during evolution. Although invertebrates have one RIM-BP protein, vertebrates have at least two RIM-BPs (RIM-BP1 and RIM-BP2), with RIM-BP3 only found in therian mammals. In contrast to the predominant expression of RIM-BP1 and RIM-BP2 in the brain, RIM-BP3 is expressed almost exclusively in the testis. Except for bioinformatic analysis data (Mittelstaedt and Schoch, 2007), little is known about the function of RIM-BP3. Here, we report that RIM-BP3 is associated with the manchette in elongating and elongated spermatids, and is essential for normal sperm morphology and male fertility. Furthermore, we find that RIM-BP3 forms complex with Hook1, which is mutated in *azh* mice.

MATERIALS AND METHODS

Mammalian expression constructs

As *RIM-BP3* is an intronless gene, the full-length coding region was PCR amplified from mouse (129/SvEv) genomic DNA and cloned into pFlag-CMV-2 (Sigma). The *Hook1* cDNA was subcloned into pcDNA3-HA from pDS-Red2-Hook1 (kindly provided by Dr Jurgen Neesen, Vienna, Austria). *Hook1*^{azh} (nucleotides 1-789) cDNA was amplified by PCR from pDS-Red2-Hook1 and cloned into pcDNA3-HA. All PCR-cloned constructs were verified by DNA sequencing.

Antibodies

For the generation of RIM-BP3 specific antibodies, PCR fragments for antigen regions (Fig. 1A) were cloned into pET-41b (+) vector (Novagen) to produce glutathione *S*-transferase (GST) fusion proteins. Antisera were raised and affinity purified as described previously (Ge et al., 2004). The monoclonal anti-α-tubulin, anti-β-actin, anti-Flag and anti-HA antibodies were from Sigma-Aldrich. The polyclonal anti-human Hook1 was from Proteintech Group. The Alexa Fluor 488 goat anti-rabbit IgG and Alexa Fluor 546 goat anti-mouse IgG were purchased from Molecular Probes.

Germ cell purification

Spermatogenic cells were isolated from adult mouse testes as described previously (Bellve, 1993). When required, discrete populations of germ cells were isolated using unit gravity sedimentation velocity in 2-4% BSA gradient (Bellve, 1993). The purity of the isolated germ cells was monitored by phase-contrast microscopy.

Western blotting analysis

Mouse tissues and purified germ cells were solubilized in the mild tissue lysis buffer as described (Herrada and Wolgemuth, 1997). The protein concentration of supernatants was determined with BioRad Assay Reagent (Bio-Rad), using BSA as the standard. Extracts were diluted in SDS-loading buffer and analyzed by standard SDS-PAGE and western blotting.

Construction of the *RIM-BP3* targeting vector

To generate the *RIM-BP3* targeting vector, DNA fragments for the 5′ and 3′ homology arms were amplified from mouse (129/SvEv) genomic DNA by PCR. The left arm consists of a 1.2 kb 5′ coding region (nucleotides 73-1248 of the *RIM-BP3* ORF) and the right arm is a 3.2 kb fragment covering the 3′ coding region of 2759 bp and the downstream UTR of 435 bp. The two arms were cloned into the pPNT vector in *Not*I-*Xho*I and *Bam*HI-*Eco*RI sites, respectively, and confirmed by sequencing.

Generation of *RIM-BP3* knockout mice

The targeting vector linearized with *Not*I was electroporated into MPI-II ES cells (129Sv/Pas derived), which were subsequently cultured in the presence of G418 and ganciclovir on mitotically inactivated MEF cells. Resistant ES cell clones were picked ~6-8 days after drug selection. Two targeted ES clones were identified from 225 clones by Southern blotting analysis using the 3′ external probe. The 3′ probe was prepared by PCR (forward, 5′-GAATATTTCGGGAGTTAAAGCATGGC-3′; reverse, 5′-CTTACAA-AGCATCATGGGAACACCAG-3′). Positive ES clones identified by Southern blotting were aggregated with CD1 (ICR) morulae for 24 hours and then transferred into pseudopregnant foster mothers. Male chimeras were bred first with ICR females to obtain mutant mice on 129Sv×ICR mixed background. The chimeras that produced high percentages of offspring with agouti fur were also bred with 129Sv/Pas females to obtain inbred mice. Heterozygotes were intercrossed to produce homozygous offspring. Mouse genotypes were identified by Southern analysis of tail DNA using 3′ external probe and by PCR using primers as follows: RIM-BP3 (+756), 5′-ATCTTTGGCAACAGCACATTCCT-3′; and RIM-BP3 (–3253), 5′-TTTCTTGGCTTGCGGTTTGGAGT-3′. Mice on mixed 129Sv×ICR genetic background were used except where indicated.

Fertility test and sperm counts

RIM-BP3$^{-/-}$ males at 8-9 weeks of age were housed with 6- to 8-week-old virgin ICR females for 2 months. The numbers and sizes of litters were recorded. Wild-type and heterozygous males were used for comparison. Females paired with homozygous males that never produced litters were subsequently placed with males of proven fertility and, if they produced a litter, were considered to be fertile and included in the study; otherwise, they were excluded. Student's *t*-test was used to compare averages in different experimental groups and $P<0.05$ was considered to be significant.

For isolation of sonication-resistant spermatid nuclei, which represent step 12 to 16 spermatids, we followed the procedure as described previously (Yu et al., 2000) with slight modifications. Briefly, the testes from two mice were homogenized in 4 ml of water containing protease inhibitors (1 mM PMSF, 1 μg/ml leupeptin and 1 μg/ml pepstatin A) using a glass-Teflon homogenizer and then sonicated for 6 minutes of total elapsed time (15 seconds on, 15 seconds off) to remove sonication-sensitive cells. Spermatid nuclei were separated from tissue debris by passing the mixture through an 80 μm mesh filter. All counts were performed using a hemacytometer.

Immunofluorescence microscopy

Squashed samples were prepared as described (Kotaja et al., 2004). Samples were then fixed sequentially in cold methanol for 10 minutes, in acetone for 30 seconds and then in PBS containing 4% paraformaldehyde for 15 minutes. After fixation, samples were permeablized with 0.5% Triton X-100 for 15 minutes and blocked for at least 1 hour at room temperature with blocking solution (PBS with 0.3% Triton X-100 and 1% BSA). Indirect immunofluorescence staining to study the localization of RIM-BP3, Hook1 and α-tubulin in testicular germ cells was carried out as described for cultured cells (Ge et al., 2004) and images of stained cells were captured with a Leica TCS SP2 laser confocal microscope.

Electron microscopy

Testes and cauda epididymides from wild-type and *RIM-BP3*$^{-/-}$ mice were examined with electron microscopy. For scanning electron microscopy of mature sperm, cauda epididymides were dissected and minced in 0.1 M phosphate buffer (pH 7.4), allowing the sperm to be released into the supernatant. The sperm were fixed in 2.5% glutaraldehyde solution in phosphate buffer, collected on poly-L-lysine-coated glass cover slips, post-fixed in osmium tetroxide, dehydrated in a

graded ethanol series, subjected to critical point drying and then coated with gold/palladium. Samples were examined with a JEOL JSM-6360LV Scanning Electron Microscope. For transmission electron microscopy, samples were fixed in 4% paraformaldehyde containing 0.05% glutaraldehyde in 0.1 M phosphate buffer, and then post-fixed in 1% osmium tetroxide. Dehydration was carried out in ethanol and the samples were embedded in Epon 812. Ultrathin sections were counterstained with uranyl acetate and lead citrate, and examined with a JEOL JEM-1230 transmission electron microscope.

Affinity purification of RIM-BP3-associated proteins

Affinity purification was carried out as described (Li et al., 2007a; Li et al., 2007b) with slight modifications. Spermatids were purified from wild-type and *RIM-BP3*$^{-/-}$ testes and lysed in lysis buffer [50 mM Tris-HCl (pH 7.4), 1 mM EDTA, 150 mM NaCl, 1% (v/v) NP-40, 0.25% (w/v) sodium deoxycholate, 1 mM DTT, 1 μg/ml aprotinin, 1 μg/ml leupeptin, 1 μg/ml pepstatin A and 1 mM PMSF]. After brief sonication, the lysates were centrifuged at 20,000 ***g*** at 4°C for 10 minutes. The supernatants were incubated with anti-RIM-BP3 (N) and anti-RIM-BP3 (C) antibodies, respectively, for 4 hours at 4°C with gentle rotation. The immuno-complex was captured by incubation with Protein A-agarose beads (GE Healthcare) at 4°C overnight with gentle rotation. The beads were washed four times with lysis buffer. Bound proteins were analyzed by SDS-PAGE and silver staining. Specific bands were excised and the protein sequence was determined using electrospray ionization LTQ tandem mass spectrometry at the Research Center for Proteome Analysis, Shanghai Institutes for Biological Sciences.

Co-immunoprecipitation

Decapsulated testes or HEK-293T cells transfected with pFlag-CMV2-RIM-BP3 and pcDNA3-HA-Hook1 or pcDNA3-HA-Hook1^{azh} were lysed in lysis buffer. Co-immunoprecipitation of RIM-BP3 and Hook1 was carried out as previously described (Xie et al., 2006). The immuno-complex was analyzed by SDS-PAGE and standard western analysis.

Yeast two-hybrid assay

For mapping the interaction regions in RIM-BP3 and Hook1, a yeast two-hybrid assay was carried out as previously described (Li et al., 2007c). RIM-BP3 fragments were cloned in-frame with the GAL4 activation domain (GAL4AD) on the prey vector pGADT7 (Clontech) and Hook1 fragments were fused with the GAL4 DNA binding domain (GAL4BD) on the bait vector pGBKT7. The bait and prey constructs were co-transformed into the yeast strain AH109 and colonies were selected and assayed on SD medium with or without adenine, His, Leu, Trp according to the recommended protocol (Clontech).

RESULTS

RIM-BP3 is specifically expressed in mouse testis, most abundantly in spermatids

Mouse *RIM-BP3* is an intronless gene encoding a large protein with 1606 amino acids. The RIM-BP3 protein has three Src homology 3 (SH3) domains and two fibronectin type III (FN3) domains in its C-terminal half (Fig. 1A). This overall organization is similar to that of RIM-BP1 and RIM-BP2 (Mittelstaedt and Schoch, 2007). In the N-terminal half, RIM-BP3 has a unique SbcC domain, which may have ATPase activity (Connelly et al., 1998; Connelly and Leach, 1996).

We examined the expression of *RIM-BP3* in adult mouse tissues by northern blotting analysis. A *RIM-BP3* transcript of about 5 kb was detected exclusively in the testis (Fig. 1B). The size of the transcript is consistent with a previous report (Mittelstaedt and Schoch, 2007). We then determined the expression of the RIM-BP3 protein in different tissues by western blotting analysis using polyclonal antibodies with validated specificity (see Fig. S1 in the supplementary material). Consistent with the northern blotting result, the RIM-BP3 protein was also detected exclusively in the testis (Fig. 1C).

In murine testis, the seminiferous epithelium undergoes postnatal development (Bellve et al., 1977; Malkov et al., 1998). We then examined the expression pattern of RIM-BP3 at various stages of this process by western analysis using testicular extracts from juvenile and adult mice (Fig. 1D). The earliest stage at which RIM-BP3 was detected was postnatal day 20, when spermatids first appear. Thereafter, the RIM-BP3 protein level increased until adulthood. Thus, RIM-BP3 is expressed most abundantly in postmeiotic germ cells.

We further investigated the types of postmeiotic germ cells that express RIM-BP3 by performing western analysis on protein extracts from purified germ cells. The purity of each type of germ cells was determined to be at least 90% by microscopic analysis (data not shown). Western blotting analysis shows that RIM-BP3 is highly expressed in elongate spermatids and weakly expressed in pachytene spermatocytes and round spermatids (Fig. 1E). Interestingly, it was detectable in residual bodies but not in mature sperm. These data show that RIM-BP3 is a testis-specific protein predominantly expressed at the haploid stage and suggest that it plays a specialized role in spermiogenesis.

The RIM-BP3 protein is associated with the manchette in developing spermatids

We then investigated subcellular distribution of RIM-BP3 in developing spermatids by performing indirect immunofluorescence analysis using squashed samples of seminiferous tubules (Kotaja et al., 2004). The expression of RIM-BP3 was first evident in step 9 spermatids, persisted until step 13 and finally disappears at step 16 (Fig. 2). In these spermatids, an extensive colocalization with the manchette was observed by co-immunostaining with anti α-tubulin antibody. The RIM-BP3 antibody is specific, as shown by the absence of signal in the knockout mouse samples (see Fig. S2 in the supplementary material). This expression pattern of RIM-BP3 correlates well with the dynamic changes of the manchette (Clermont et al., 1993), suggesting a specialized role for RIM-BP3 in the development of late-stage spermatids.

Targeted disruption of the *RIM-BP3* gene results in male infertility

To investigate the role of RIM-BP3 during spermiogenesis, we disrupted its function in mice by gene targeting. In the targeted allele, the entire sequence encoding the SbcC domain was replaced by a cassette of the *PGK*-neomycin resistance gene (Fig. 3A). The generation of mutant mice was confirmed by PCR and southern blotting analysis of tail genomic DNA (Fig. 3B). Western analysis with two different antibodies confirmed the absence of the RIM-BP3 protein in the testis of mutant mice (Fig. 3C).

Interbreeding of heterozygous mice yielded an expected Mendelian ratio (39:92:44) of *RIM-BP3*$^{+/+}$, *RIM-BP3*$^{+/-}$ and *RIM-BP3*$^{-/-}$ in F2 offspring on 129Sv×ICR genetic background, suggesting that the *RIM-BP3* deficiency caused no embryonic lethality. Adult mutant mice were normal in appearance, health and developed with no identifiable anatomical or behavioral abnormalities. Given the expression of RIM-BP3 in the testis, we studied fertility in *RIM-BP3*-null mice by mating them with wild-type females. The mutant males were found to be infertile, although they were sexually active and produced vaginal plugs in female partners. Over a 2-month period of continuous mating, only one female became pregnant and gave birth to one pup (Table 1). The heterozygous males showed normal fertility and produced normal litter sizes (Table 1 and data not shown). To determine whether the poor reproductive performance of homozygous males was due to a failure of fertilization, they were mated with

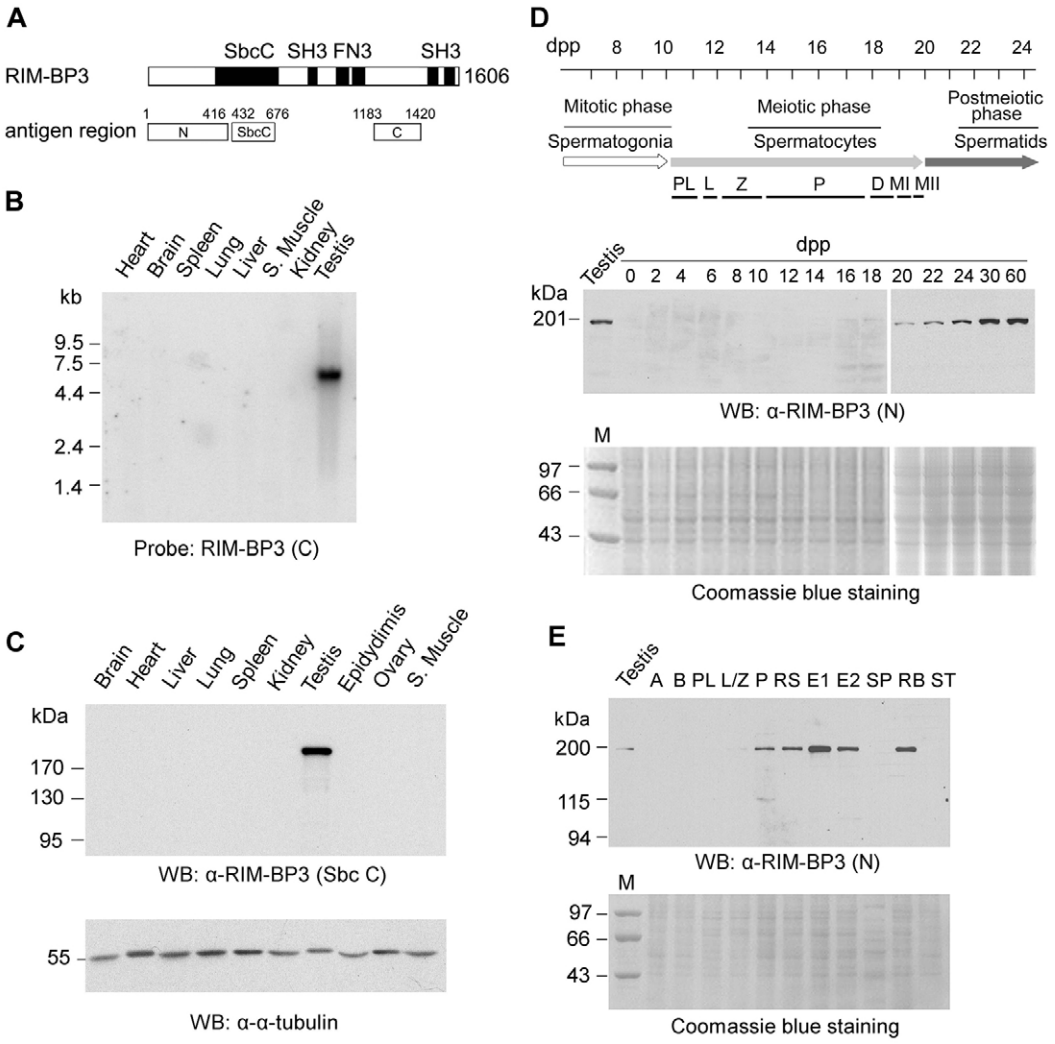

Fig. 1. Specific expression of RIM-BP3 in the mouse testis. (**A**) The RIM-BP3 protein showing the conserved domains and three antigen regions for raising antibodies. (**B**) Northern hybridization analysis of the *RIM-BP3* transcript in different tissues as indicated above. The mRNA blot (Clontech) contains 2 μg mRNA on each lane. The hybridization probe corresponds to the C-terminal coding sequence (nucleotides 3547-4260). (**C**) Western analysis of the RIM-BP3 protein in different tissues as indicated above. The detection of α-tubulin serves as a loading control (lower panel). (**D**) Western detection of the RIM-BP3 protein in developing postnatal testis. Upper panel, diagram of stages of mouse spermatogenesis; PL, preleptotene spermatocytes; L, leptotene spermatocytes; Z, zygotene spermatocytes; P, pachytene spermatocytes; D, diplotene spermatocytes; MI, meiosis I; MII, meiosis II; middle panel, western analysis of RIM-BP3 (0-60 days post partum); bottom panel, Coomassie blue staining of the protein samples. (**E**) Western detection of RIM-BP3 in purified male germ cells. A, type A spermatogonia; B, type B spermatogonia; RS, round spermatids; E1 and E2, two pools of elongate spermatids; SP, mature sperm; RB, residual bodies; ST, Sertoli cells. Other abbreviations used are as in D. The lower panel shows Coomassie blue staining of samples used for the western analysis.

superovulated normal females. Eggs were collected from the ampullae of the oviducts of mated females and scored for fertilization based on the presence of a male pronucleus (Borghei et al., 2006). We observed that 92.4% eggs harvested from the females plugged by wild-type males were fertilized. By contrast, only 9.3% eggs harvested from the females plugged by *RIM-BP3*$^{-/-}$ males were fertilized (see Table S1 in the supplementary material). These data reveal that the ability of *RIM-BP3*$^{-/-}$ males to fertilize eggs in vivo was severely compromised. In addition, this abnormality was not dependent on genetic background, as a lower fertilization rate (2%) by the mutant males was also observed in pure 129Sv strains.

To determine whether the failure of fertilization is associated with reduced quantity and quality of the sperm, we examined the reproductive organs and sperm numbers in testis and epididymis. The weights of seminal vesicle, testis and cauda epididymis of mutant mice were comparable with those of their wild-type and heterozygous

Table 1. Fecundity of *RIM-BP3*-deficient males during an 8-week mating period

Genetic background	*RIM-BP3* genotype	Number fertile/total	Litters per fertile pair (mean±s.e.m.)	Mean litter size (mean±s.e.m.)
129sv×ICR	+/+	10/10	2.7±0.2	12.8±1.3
	+/–	10/10	2.9±0.1	13.5±0.8
	–/–	1/10	1	1

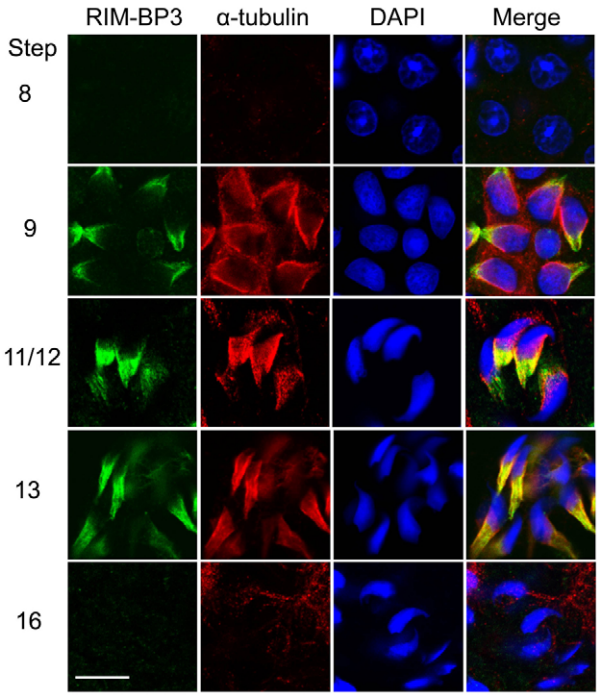

Fig. 2. Distribution of the RIM-BP3 protein in elongating spermatids. Testicular germ cells were prepared from adult wild-type mice, and indirect immunofluorescence staining was performed using polyclonal anti-RIM-BP3 SbcC (green) and monoclonal anti-α-tubulin (red) antibodies. The slides were counterstained with DAPI to visualize the nucleus. Testicular germ cells from *RIM-BP3* knockout mice were used as negative controls (see Fig. S2 in the supplementary material). Scale bar: 10 μm.

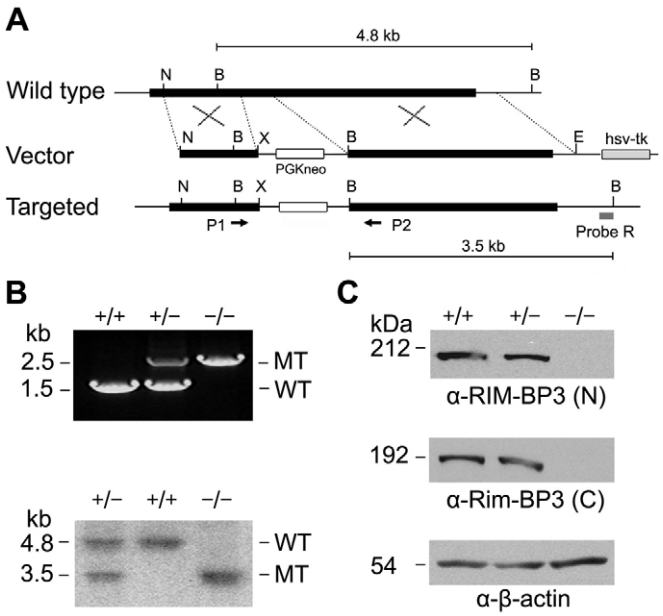

Fig. 3. Targeted disruption of the *RIM-BP3* gene. (**A**) The strategy for the generation of a targeted *RIM-BP3* allele. Black bars represent coding regions of the single-exon gene. *Bam*HI restriction sites (B) and the probe used for Southern analysis (R), and PCR primers (arrows) used for genotyping are indicated. (**B**) Genotype confirmation of the knockout mouse by PCR (upper panel) and Southern analysis (lower panel). The DNA fragments derived from the wild-type (WT) and mutant (MT) alleles are indicated on the right. +/+, wild type; +/–, heterozygote; –/–, homozygote. (**C**) Genotype confirmation of the knockout mouse by western analysis. The blot containing testis protein extracts from wild-type (+/+), heterozygous (+/–) and homozygous (–/–) adult mice was probed with antibodies specific for N- and C-terminal regions (Fig. 1A). The detection of β-actin serves as a loading control.

littermates (Table 2), indicating normal development. The number of sonication-resistant spermatid nuclei (step 12-16 spermatids) in testis was also normal. However, caudal epididymal sperm counts decreased by one-third (Table 2), indicating that sperm production or the release of mature sperm from the testis might be affected. Histology of seminiferous tubules did not reveal any gross morphological abnormality in mutant mice, except for deformities of spermatid nuclei (see Fig. S3D, inset in the supplementary material).

Abnormal morphology of mature epididymal sperm from *RIM-BP3* mutant mice

Although the amount of sperm in the cauda epididymis was slightly reduced in *RIM-BP3*$^{-/-}$ mice compared with the wild-type counterpart, mutant males were nearly sterile. To determine the basis for drastically reduced fertility in the mutant mice, sperm were obtained from the cauda epididymis and analyzed by electron microscopy. Scanning electron microscopy demonstrated that nearly all sperm from *RIM-BP3*$^{-/-}$ mice displayed abnormal head morphology, lacking a typical hook-shaped appearance (Fig. 4A, parts a-c) – a feature often related to nuclear shaping defects. Moreover, a high number of sperm had flagella detached from the head and some flagella showed various degrees of bending. To further characterize the inner structure of the abnormal sperm, we carried out transmission electron microscope (TEM) analysis (Fig. 4B). As expected, deformed nuclei were observed in *RIM-BP3*$^{-/-}$ mice. Interestingly, about 90% of sperm also showed detached acrosome and expanded perinuclear space.

Spermiogenesis is impaired in *RIM-BP3* mutant mice

Disruption of *RIM-BP3* in mice caused male infertility owing to abnormal sperm heads. To characterize the morphological defects in the developing germ cells in detail, we performed transmission electron microscopic study of testis sections. The histological

Table 2. Organ weights and numbers of sperm in *RIM-BP3*-deficient mice*

RIM-BP3 genotype	Seminal vesicle (mg)	Testis weight (mg)	Cauda epididymis weight (mg)	Sperm heads per mg testis (10^4)	Sperm per mg cauda epididymis (10^4)
+/+	314±11	129±3	38±2	21±1	85±5
+/–	296±12	127±4	27±1	20±1	79±4
–/–	270±6	131±6	26±1	18±1	57±5

*Mice (n=10) were used at 12 weeks of age. All values are means and standard error of mean (s.e.m.).

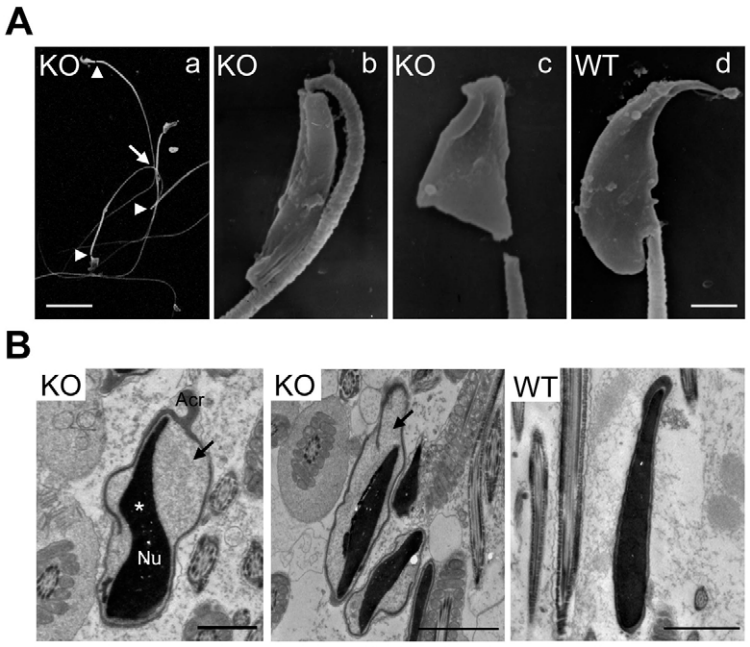

Fig. 4. Morphological abnormalities of epididymal sperm from *RIM-BP3* knockout mice. (**A**) Scanning electron micrographs. (a) Abnormal head shaping, tail detachment (arrowheads) and bending (arrow) occur in sperm of the mutant mouse. Scale bar: 20 μm. (b,c) Higher magnification of abnormal spermatid heads lacking the hook-shaped appearance typical of a normal spermatid from the wild-type mouse (d). Scale bar in d: 2 μm in b-d. (**B**) Transmission electron micrographs. Deformed nuclei were observed (asterisk) and most of the sperm heads in mutant mice display a detached acrosome (black arrow). Acr, acrosome; Nu, nucleus. Scale bars: 1 μm.

analysis of the seminiferous tubules above revealed spermatogonia, spermatocytes and Sertoli cells with normal morphology, whereas spermatids of step 12 displayed deformed nuclei (see Fig. S3 in the supplementary material). This observation was confirmed by transmission electron microscopic analysis. The spermatids from *RIM-BP3*-deficient mice displayed various defects in the acrosome, acroplaxome, manchette and nucleus. The earliest abnormality was seen occasionally in step 5 round spermatids. Proacrosomal vesicles derived from Golgi apparatus could not fuse to form a single large acrosomal vesicle and the acroplaxome was bent at several sites (Fig. 5B). However, from a structural point of view, elongating and elongated spermatids were the most affected with a variety of abnormalities. About 10% of elongate spermatids showed discontinuity of acrosome in the plane of section (arrowhead in Fig. 5D,F,K). This occurrence was a consequence of a deficient fusion of proacrosomal vesicles during the early stages of acrosome biogenesis. Moreover, the acroplaxome was severely deformed. As a consequence, the acrosome was misplaced and the outline of the nucleus under the acroplaxome was irregular (Fig. 5F,G). As spermatid elongation proceeded across step 10/11, abnormal development of the manchette could be clearly seen. The manchette in *RIM-BP3*-null spermatids presented symmetric development with a conical shape (Fig. 5F) and, in appropriate sections, invagination of membrane-bound microtubules could be observed (Fig. 5H). Some elongated spermatids also showed an abnormal positioning of the perinuclear ring anterior to the marginal ring of the acroplaxome. Consequently, the manchette covers a part of the acrosome (Fig. 5I). At the end of spermiogenesis, the majority of condensed spermatids exhibited detached acrosome, deformed nucleus and expanded perinuclear space with some unidentified materials (Fig. 5K,L).

We further confirmed ectopic positioning of manchette in elongating spermatids of *RIM-BP3*$^{-/-}$ mice by indirect immunofluorescence analysis using anti α-tubulin antibody. Consistent with TEM analysis, the manchette became abnormal in elongating *RIM-BP3*-deficient spermatids (see Fig. S4, left in the supplementary material). At the early stage of differentiation (step 9), the spermatids of mutant mice had a normal bell-shaped manchette covering a typical ovoid-shaped nucleus. However, by step 11/12, the manchette and nucleus of most mutant spermatids had conically symmetric caudal ends that were different from the asymmetric ones of wild-type spermatids. In addition, the manchette oriented parallel to the longitudinal axis of the mutant spermatid head, whereas in the normal spermatids the manchette oriented at 45° to the principal axis of the spermatid head (see Fig. S4, right in the supplementary material).

The RIM-BP3 protein interacts with Hook1

In order to uncover the molecular consequences of the lack of RIM-BP3 in spermiogenesis, we set out to identify RIM-BP3-associated protein(s) in spermatids. Immunoprecipitation with two different RIM-BP3 antibodies pulled down a prominent protein (about 100 kDa) co-purified from wild-type spermatids, but not from *RIM-BP3*-deficient spermatids (Fig. 6A). Mass spectrometry analysis revealed that the co-purified protein is Hook1, a manchette-associated protein in developing spermatids (Mendoza-Lujambio et al., 2002). The confirmation of Hook1 as an interacting protein was provided by performing a co-immunoprecipitation (Co-IP) assay on whole testis extracts. Hook1 was detected by western analysis in the immunoprecipitated proteins obtained with anti-RIM-BP3 antibody from wild-type but not from the *RIM-BP3*-deficient testis extract (Fig. 6B).

To define domains responsible for the interaction, we constructed a series of deletion mutants of both proteins for yeast two-hybrid assays. We found that yeast expressing the C-terminal part (amino acids 830-1606) of RIM-BP3 could grow on the selective medium (Fig. 6C), indicating that this region containing the SH3 and FNIII domains is required for the interaction with Hook1. Similarly, we mapped the interaction region in Hook1. We found that only the coiled-coil domain (amino acids 165-661) enabled yeast cells to grow on the selective medium, though more slowly than the yeast expressing the full-length Hook1 (Fig. 6D). These findings indicate that a large part of Hook1, including the coiled-coil domain is involved in the interaction with RIM-BP3.

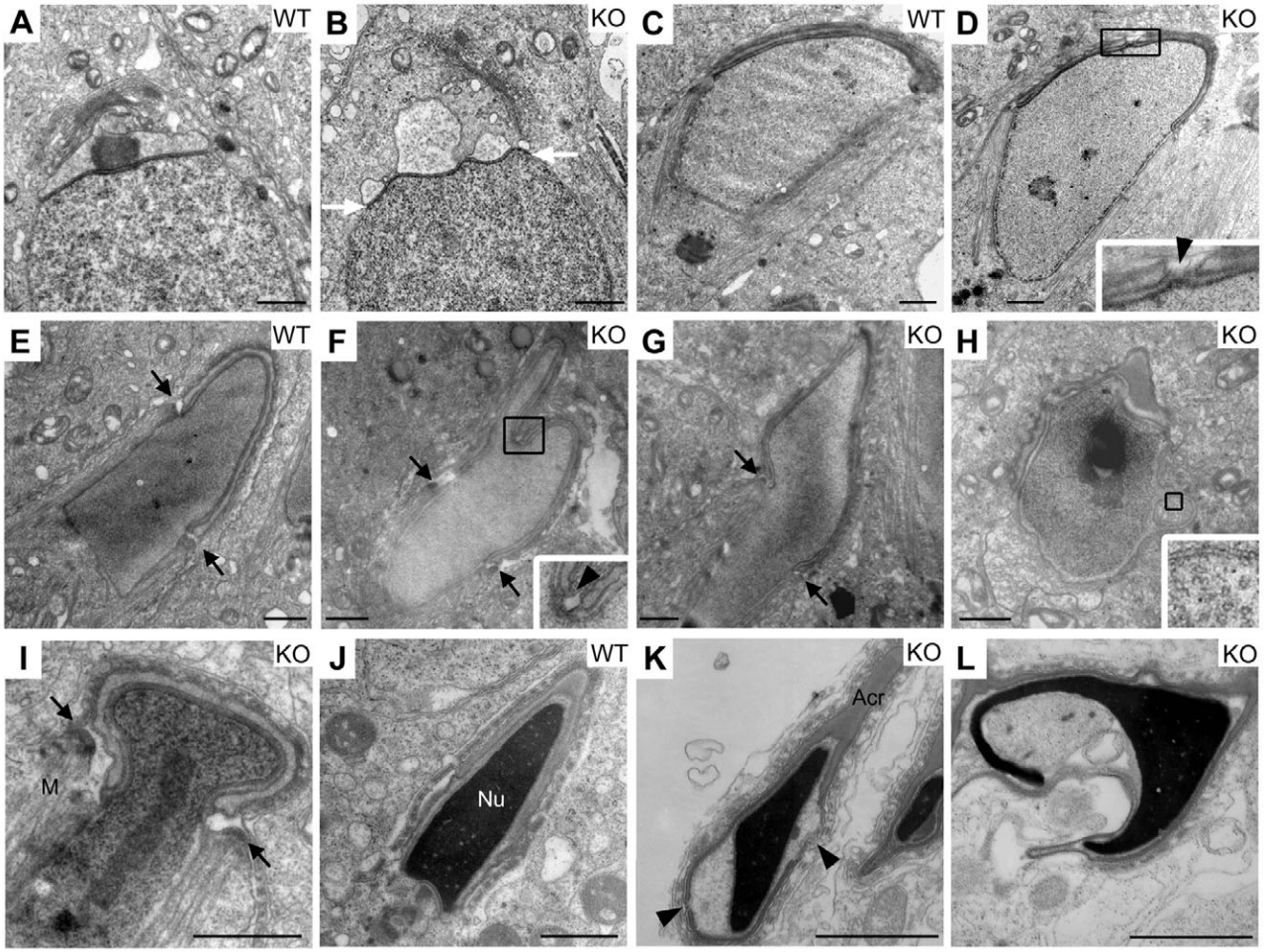

Fig. 5. Spermiogenesis abnormalities in *RIM-BP3* knockout mice revealed by transmission electron microscopy. (**A**,**B**) Step 5 spermatids. Unfused proacrosomal vesicles are aligned above the bent acroplaxome in a mutant round spermatid (B). The ends of the extending acroplaxome in this section are marked with white arrows. (**C**,**D**) Step 9 spermatids. Acrosome fragmentation was occasionally observed in mutant elongating spermatids as shown in D. The breakage point is indicated with an arrowhead (D, inset). (**E-G**) Step 10/11 spermatids. At this elongating stage, abnormalities ranged from acrosome discontinuity (F, inset, arrowhead), acroplaxome distortion (F,G) and nuclear shape irregularity to symmetric manchette appearance with a conical shape (F). Black arrows indicate the perinuclear ring of the machette. (**H**,**I**) Step 12/13 spermatids. A membrane-bound microtubular bundle is ectopically located within the nuclear envelope on the presented cross-section (H, inset). The perinuclear ring (I, left arrow) at the left is shifted away from its normal location subjacent to the marginal ring (compare with the perinuclear ring on the right, arrow). (**J-L**) Step 15/16 spermatids. The mutant elongated spermatids frequently contain deformed nucleus and detached acrosome, with some unidentified materials in the expanded perinuclear space. Acrosome gaps (arrowheads, K) continue to exist. Nu, nucleus; Acr, acrosome; M, manchette. Scale bars: 1 μm.

Mutation of Hook1 in *azh* mice disrupts interaction with RIM-BP3

Electron microscopy and immunostaining analyses revealed aberrant manchettes in *RIM-BP3* deficient spermatids (Fig. 5 and see Fig. S4 in the supplementary material). These abnormalities are reminiscent of those observed in *azh* mutant mice, in which a deletion of a 2 kb genomic sequence of the *Hook1* gene leads to truncation of the entire C-terminal part (Cole et al., 1988; Mendoza-Lujambio et al., 2002) (Fig. 7A). Based on the physical association of RIM-BP3 and Hook1 in vivo and in vitro, we reasoned that the truncated Hook1^{azh} might lose interaction with RIM-BP3, which could be an underlying mechanism for the ectopic positioning of the manchette. Therefore, co-immunoprecipitation was carried out with the two proteins expressed in transfected 293T cells. Indeed, we found that the mutant Hook1 had lost its ability to interact with RIM-BP3 (Fig. 7B).

DISCUSSION

In the present study, we demonstrate that RIM-BP3 is a testis-specific protein predominantly expressed at the haploid stage and is important for spermiogenesis. Targeted disruption of the *RIM-BP3* gene results in male infertility without other identifiable anatomical or behavioral abnormalities. The infertility of the *RIM-BP3* knockout males is ascribed to the severe malformation of sperm heads. The sperm heads of knockout males lack the typical hook-shaped appearance and have deformed nucleus and enlarged perinuclear space, indicative of a defective nuclear shaping.

Spermiogenesis is an intricate process by which a round haploid spermatid cell differentiates into a mature elongated spermatozoon. There are multiple mechanisms proposed to ensure the correct formation and organization of specialized structures of a mature spermatozoon (Meistrich, 1993; Toshimori and Ito, 2003). The acrosome-acroplaxome-manchette complex was proposed to play a

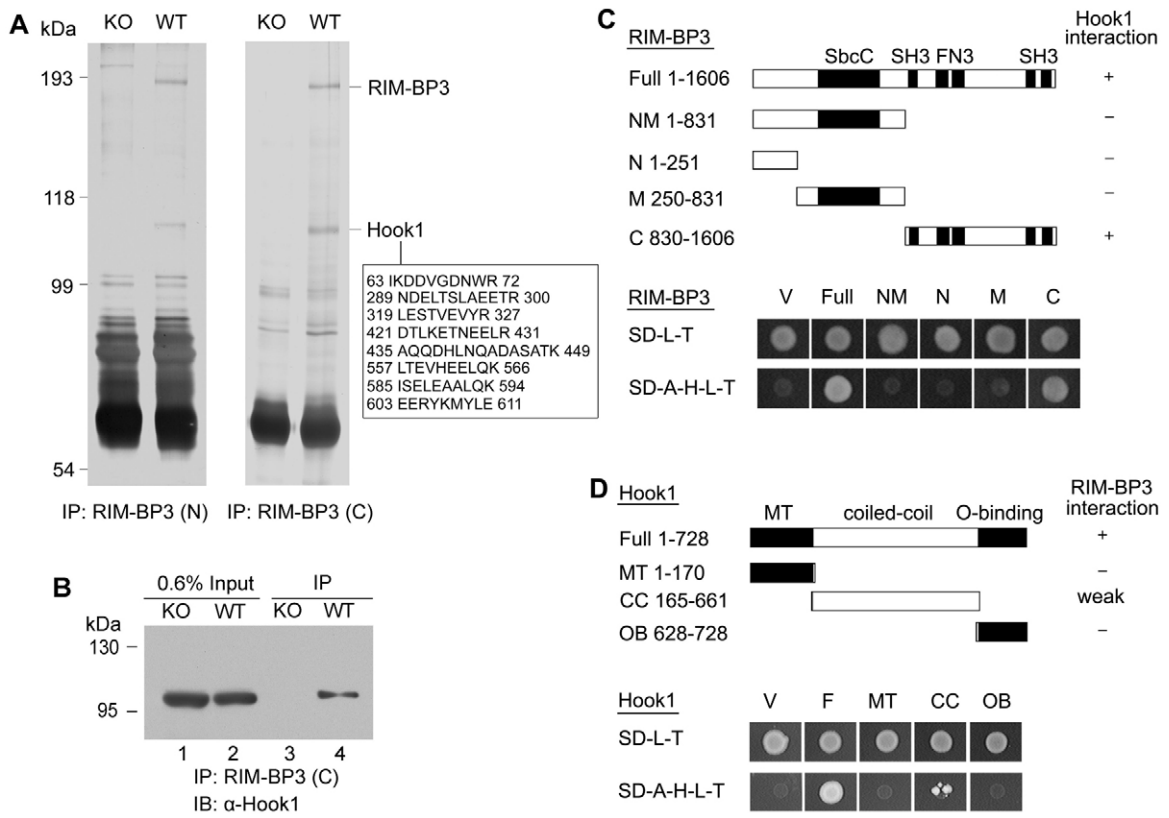

Fig. 6. The RIM-BP3 protein is associated with Hook1. (**A**) Purification and identification of proteins associated with RIM-BP3. Protein extracts of spermatids isolated from wild-type (WT) mice and *RIM-BP3* knockout (KO) mice were immunoprecipitated with anti-RIM-BP3 (N) or anti-RIM-BP3 (C) antibody. The immunoprecipitated proteins were separated by SDS-PAGE and visualized by silver staining. The prominent protein specifically co-purified with RIM-BP3 was identified as Hook1 by mass spectrometric analysis. The detected Hook1 peptides are listed in the box, with their amino acid positions indicated. (**B**) Co-immunoprecipitation of endogenous RIM-BP3 and Hook1. The total testicular extracts from *RIM-BP3* knockout (lane 3) and wild-type mice (lane 4) were immunoprecipitated with the anti-RIM-BP3 (C) antibody. The immunoprecipitates were fractionated by SDS-PAGE and blotted with anti-Hook1 antibody. Left two lanes are 0.6% of the input extracts used for immunoprecipitation. (**C**) Mapping of the interaction region in RIM-BP3 by yeast two-hybrid assay. RIM-BP3 full-length and its four fragments (upper panel) were fused to GAL4AD and co-transformed into yeast with the bait construct GAL4BD-Hook1. The interaction capability of each fragment was judged by the appearance of colonies on the SD minimal medium (SD-L-T-A-H) (lower panel). (**D**) Mapping of the interaction region in Hook1 by yeast two-hybrid assay. Full-length Hook1 and its three fragments (upper panel) were fused to GAL4BD and co-transformed into yeast with the prey construct GAL4AD-RIM-BP3. Growth of colonies on the SD minimal medium (SD-L-T-A-H) reflects positive interaction (lower panel). MT, microtubule-binding domain; O-binding, organelle-binding domain (Mendoza-Lujambio et al., 2002).

major role in nuclear shaping (Kierszenbaum and Tres, 2004). In wild-type spermatids, the acrosome is tightly bound to the acroplaxome plate, which in turn is anchored to the nuclear envelope of the elongating spermatid nucleus. The acroplaxome may provide a scaffold to modulate exogenous constriction forces generated by Sertoli cell F-actin hoops during spermatid head elongation. The manchette is composed of bundles of microtubules that emerge from the perinuclear ring, which is organized subjacent to the marginal ring of the acroplaxome. Both the marginal ring and the perinuclear ring reduce their diameter along with the elongation of the spermatid nucleus (Kierszenbaum and Tres, 2004). Our finding that targeted disruption of *RIM-BP3* resulted in complex abnormalities in the acrosome-acroplaxome-manchette complex in association with sperm head deformity underscores the importance of this complex in spermiogenesis. The variable anomalies include: (1) deficient tethering and fusion of proacrosomal vesicles in round spermatids, which results in the discontinuities of the acrosome in elongating and elongated spermatids; (2) distorted acroplaxome plate and misplaced acrosome; (3) malformed manchette in elongate spermatids such as the appearance in a symmetric conical shape, invagination into the nucleus and the ectopic positioning of the perinuclear ring anterior to the marginal ring. These perturbations in acrosome-acroplaxome-manchette complex are conceivably the major causes for malformation of spermatid heads.

So how does the acrosome-acroplaxome-manchette complex become abnormal? Given the localization of the RIM-BP3 protein in the manchette in normal spermatids, alteration in the distribution of the manchette microtubules might represent one of the initial events in *RIM-BP3*-deficient spermatids. Consistent with this idea, spermatid deformation owing to aberrant development or ectopic positioning of the manchette was also observed in knockout mice deficient in E-MAP-115, a microtubule-stabilizing protein (Komada et al., 2000) and CLIP-170, a microtubule plus-end-tracking protein (Akhmanova et al., 2005) as well as in animals treated with microtubule-disrupting agents such as colchicine and carbendazim (Handel, 1979; Nakai et al., 1998).

The role of RIM-BP3 in the control of microtubule organization might be mediated by Hook1. We have demonstrated that Hook1 is stably associated with RIM-BP3 in elongate spermatids. Hook1 contains a microtubule-binding domain in its N-terminal part and an

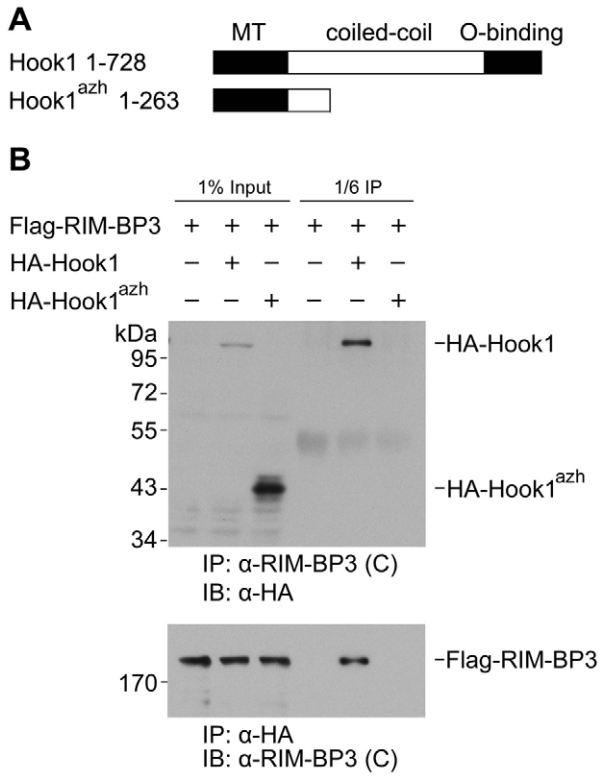

Fig. 7. The Hook1 *azh* mutant is unable to interact with RIM-BP3. (**A**) Schematic representation of the wild-type Hook1 and the *azh* mutant Hook1 protein (Hook1^{azh}) with their polypeptide length indicated. (**B**) The expression constructs of Flag-RIM-BP3, HA-Hook1 and HA-Hook1^{azh} were co-transfected into HEK-293T cells with various combinations indicated at the top. Whole-cell extracts were immunoprecipitated with the anti-RIM-BP3 (C) or anti-HA antibody, and the precipitated proteins were analyzed by western blotting using anti-HA or anti-RIM-BP3 (C) antibody as indicated.

organelle-binding domain in the C-terminal region. This domain organization may allow Hook1 to establish a link between the manchette microtubules and other cellular organelles, e.g. the nuclear envelope (Mendoza-Lujambio et al., 2002). *RIM-BP3*-deficient spermatids often show the ectopic positioning of manchette, whereas Hook1 remains associated to the malformed manchette (Fig. 5; see Fig. S4 in the supplementary material). This suggests that RIM-BP3 has no effect on the binding of Hook1 to the manchette. Rather, it may modulate the interaction of Hook1 with certain organelles to which the manchette should be anchored. Interestingly, the phenotypes of *RIM-BP3*-deficient mice, such as abnormal sperm heads, detached tails and aberrant manchette positioning, are very similar to those of *azh/azh* mice, which are caused by loss of Hook1 function (Cole et al., 1988; Mendoza-Lujambio et al., 2002; Mochida et al., 1999). In *azh/azh* mice, exons 10 and 11 in the *Hook1* gene are deleted, resulting in a truncated protein containing only the microtubule-binding domain and a small part of the coiled-coil domain (Mendoza-Lujambio et al., 2002). Consistent with requirement of the coiled-coil domain for the interaction with RIM-BP3 (Fig. 6D), the truncated Hook1^{azh} mutant protein has lost the ability to interact with RIM-BP3 (Fig. 7). As the microtubule-binding domain is intact in Hook1^{azh}, we assume that the *azh/azh* phenotype related to the manchette might arise due to abolished interaction of Hook1 with RIM-BP3. The overall phenotypic similarity of *azh/azh* and *RIM-BP3*$^{-/-}$ mice could reflect the importance of the interaction between Hook1 and RIM-BP3 in positioning the manchette along the nuclear surface. As an adaptor molecule, RIM-BP3 might link with the manchette through Hook1 to ensure correct positioning of the manchette. The disruption of a common pathway involving Hook1 and RIM-BP3 might be responsible for the abnormal spermatid development observed in both *azh* and *RIM-BP3* mutant mice.

As a large multidomain protein, RIM-BP3 may also have a functional role in the manchette besides its contribution to manchette development. We observed an accumulation of unidentified materials in the enlarged perinuclear region of some elongated spermatids of *RIM-BP3* mutant mice (Fig. 5K,L). This provides a clue that RIM-BP3 might be involved in intramanchette transport. Loss of RIM-BP3 might affect nucleocytoplasmic exchanges owing to defective intramanchette transport. This might in turn lead to the retention of residual materials around the nucleus of late-stage spermatids, which would normally be transported to cytoplasmic droplets. The presence of residual materials may consequently impair the tight association of the acrosome and manchette with the nuclear membrane, causing their detachment and thus expanded perinuclear space. Moreover, abnormal tethering and fusion of proacrosomal vesicles along the acroplaxome seen in early round spermatids could be due to a deficiency in vesicle transport caused by RIM-BP3 depletion. In support of this potential role of RIM-BP3 in intramanchette transport, KIF3B, a kinesin family member, was identified as a RIM-BP3 interacting partner in a yeast two-hybrid screen (data not shown). Kinesins are microtubule-based molecular motors responsible for intramanchette transport (Kierszenbaum, 2002). KIFC1, another kinesin member that associates with a complex containing nucleoporin NUP62, has been implicated in acrosome/manchette transport along the nuclear membrane (Yang et al., 2006). Further circumstantial evidence comes from the fact that both RIM-BP1 and RIM-BP2, the two highly conserved parologs that are expressed in the brain, are involved in vesicle transport in neuronal cells (Hibino et al., 2002). Finally, both RIM-BP3 interacting partners Hook1 and KIF3B have been connected with Rab proteins involved in endocytosis (Imamura et al., 2003; Luiro et al., 2004). All these proteins, including RIM-BP3, Hook1, Kinesins, RIMs and Rabs, seem to be networked for complex intracellular trafficking and transport.

The highly conserved human RIM-BP3 protein is expected to have similar function in spermiogenesis. Human male infertility is often related to abnormal spermatozoon head shape (Baccetti et al., 1989; Baccetti et al., 1984; Toyama et al., 2000; Toyama et al., 1995). Although so far there is no report of infertile men with mutations on chromosome 22q11.21, where the three copies of the human *RIM-BP3* gene are located, our study in the mouse suggests that the human *RIM-BP3* could serve as a candidate gene for mutational analysis in infertile individuals with teratozoospermia.

We thank A. Kierszenbaum and Y. Zhang for advice on the work, X. Zhang for help with electron microscopy and J. Neesen for the *Hook1* cDNA. This work was supported by grants from the Ministry of Science and Technology (2007CB947503, 2005CB522400) and the National Science Foundation of China (30671187). We also thank the Max-Planck Society and the Dr H. Storz Stiftung for support.

Supplementary material

Supplementary material for this article is available at http://dev.biologists.org/cgi/content/full/136/3/373/DC1

References

Akhmanova, A., Mausset-Bonnefont, A. L., van Cappellen, W., Keijzer, N., Hoogenraad, C. C., Stepanova, T., Drabek, K., van der Wees, J., Mommaas, M., Onderwater, J. et al. (2005). The microtubule plus-end-tracking protein CLIP-170 associates with the spermatid manchette and is essential for spermatogenesis. *Genes Dev.* **19**, 2501-2515.

Baccetti, B., Selmi, M. G. and Soldani, P. (1984). Morphogenesis of 'decapitated' spermatozoa in a man. *J. Reprod. Fertil.* **70**, 395-397.
Baccetti, B., Burrini, A. G., Collodel, G., Magnano, A. R., Piomboni, P., Renieri, T. and Sensini, C. (1989). Morphogenesis of the decapitated and decaudated sperm defect in two brothers. *Gamete Res.* **23**, 181-188.
Bellve, A. R. (1993). Purification, culture, and fractionation of spermatogenic cells. *Methods Enzymol.* **225**, 84-113.
Bellve, A. R., Cavicchia, J. C., Millette, C. F., O'Brien, D. A., Bhatnagar, Y. M. and Dym, M. (1977). Spermatogenic cells of the prepuberal mouse. Isolation and morphological characterization. *J. Cell Biol.* **74**, 68-85.
Borghei, A., Ouyang, Y. B., Westmuckett, A. D., Marcello, M. R., Landel, C. P., Evans, J. P. and Moore, K. L. (2006). Targeted disruption of tyrosylprotein sulfotransferase-2, an enzyme that catalyzes post-translational protein tyrosine O-sulfation, causes male infertility. *J. Biol. Chem.* **281**, 9423-9431.
Clermont, Y., Oko, R. and Hermo, L. (1993). Cell biology of mammalian spermiogenesis. In *Cell and Molecular Biology of the Testis* (ed. C. Desjardins and L. L. Ewing), pp. 332-376. New York: Oxford University Press.
Cole, A., Meistrich, M. L., Cherry, L. M. and Trostle-Weige, P. K. (1988). Nuclear and manchette development in spermatids of normal and azh/azh mutant mice. *Biol. Reprod.* **38**, 385-401.
Connelly, J. C. and Leach, D. R. (1996). The sbcC and sbcD genes of Escherichia coli encode a nuclease involved in palindrome inviability and genetic recombination. *Genes Cells* **1**, 285-291.
Connelly, J. C., Kirkham, L. A. and Leach, D. R. (1998). The SbcCD nuclease of Escherichia coli is a structural maintenance of chromosomes (SMC) family protein that cleaves hairpin DNA. *Proc. Natl. Acad. Sci. USA* **95**, 7969-7974.
Escalier, D., Silvius, D. and Xu, X. (2003). Spermatogenesis of mice lacking CK2alpha': failure of germ cell survival and characteristic modifications of the spermatid nucleus. *Mol. Reprod. Dev.* **66**, 190-201.
Fuhrmann, G., Chung, A. C., Jackson, K. J., Hummelke, G., Baniahmad, A., Sutter, J., Sylvester, I., Scholer, H. R. and Cooney, A. J. (2001). Mouse germline restriction of Oct4 expression by germ cell nuclear factor. *Dev. Cell* **1**, 377-387.
Ge, Y. Z., Pu, M. T., Gowher, H., Wu, H. P., Ding, J. P., Jeltsch, A. and Xu, G. L. (2004). Chromatin targeting of de novo DNA methyltransferases by the PWWP domain. *J. Biol. Chem.* **279**, 25447-25454.
Handel, M. A. (1979). Effects of colchicine on spermiogenesis in the mouse. *J. Embryol. Exp. Morphol.* **51**, 73-83.
Herrada, G. and Wolgemuth, D. J. (1997). The mouse transcription factor Stat4 is expressed in haploid male germ cells and is present in the perinuclear theca of spermatozoa. *J. Cell Sci.* **110**, 1543-1553.
Hibino, H., Pironkova, R., Onwumere, O., Vologodskaia, M., Hudspeth, A. J. and Lesage, F. (2002). RIM binding proteins (RBPs) couple Rab3-interacting molecules (RIMs) to voltage-gated Ca^{2+} channels. *Neuron* **34**, 411-423.
Imamura, T., Huang, J., Usui, I., Satoh, H., Bever, J. and Olefsky, J. M. (2003). Insulin-induced GLUT4 translocation involves protein kinase C-lambda-mediated functional coupling between Rab4 and the motor protein kinesin. *Mol. Cell. Biol.* **23**, 4892-4900.
Kang-Decker, N., Mantchev, G. T., Juneja, S. C., McNiven, M. A. and van Deursen, J. M. (2001). Lack of acrosome formation in Hrb-deficient mice. *Science* **294**, 1531-1533.
Kierszenbaum, A. L. (2002). Intramanchette transport (IMT): managing the making of the spermatid head, centrosome, and tail. *Mol. Reprod. Dev.* **63**, 1-4.
Kierszenbaum, A. L. and Tres, L. L. (2004). The acrosome-acroplaxome-manchette complex and the shaping of the spermatid head. *Arch. Histol. Cytol.* **67**, 271-284.
Kierszenbaum, A. L., Rivkin, E. and Tres, L. L. (2007). Molecular biology of sperm head shaping. *Soc. Reprod. Fertil.* **65 Suppl.**, 33-43.
Komada, M., McLean, D. J., Griswold, M. D., Russell, L. D. and Soriano, P. (2000). E-MAP-115, encoding a microtubule-associated protein, is a retinoic acid-inducible gene required for spermatogenesis. *Genes Dev.* **14**, 1332-1342.
Kotaja, N., Kimmins, S., Brancorsini, S., Hentsch, D., Vonesch, J. L., Davidson, I., Parvinen, M. and Sassone-Corsi, P. (2004). Preparation, isolation and characterization of stage-specific spermatogenic cells for cellular and molecular analysis. *Nat. Methods* **1**, 249-254.
Kramer, H. and Phistry, M. (1996). Mutations in the Drosophila hook gene inhibit endocytosis of the boss transmembrane ligand into multivesicular bodies. *J. Cell Biol.* **133**, 1205-1215.
Kramer, H. and Phistry, M. (1999). Genetic analysis of hook, a gene required for endocytic trafficking in drosophila. *Genetics* **151**, 675-684.
Li, B., Zhou, J., Liu, P., Hu, J., Jin, H., Shimono, Y., Takahashi, M. and Xu, G. (2007a). Polycomb protein Cbx4 promotes SUMO modification of de novo DNA methyltransferase Dnmt3a. *Biochem. J.* **405**, 369-378.
Li, J. Y., Pu, M. T., Hirasawa, R., Li, B. Z., Huang, Y. N., Zeng, R., Jing, N. H., Chen, T., Li, E., Sasaki, H. et al. (2007b). Synergistic function of DNA methyltransferases Dnmt3a and Dnmt3b in the methylation of Oct4 and Nanog. *Mol. Cell. Biol.* **27**, 8748-8759.
Li, Y. Q., Zhou, P. Z., Zheng, X. D., Walsh, C. P. and Xu, G. L. (2007c). Association of Dnmt3a and thymine DNA glycosylase links DNA methylation with base-excision repair. *Nucleic Acids Res.* **35**, 390-400.
Luiro, K., Yliannala, K., Ahtiainen, L., Maunu, H., Jarvela, I., Kyttala, A. and Jalanko, A. (2004). Interconnections of CLN3, Hook1 and Rab proteins link Batten disease to defects in the endocytic pathway. *Hum. Mol. Genet.* **13**, 3017-3027.
Malkov, M., Fisher, Y. and Don, J. (1998). Developmental schedule of the postnatal rat testis determined by flow cytometry. *Biol. Reprod.* **59**, 84-92.
Martianov, I., Brancorsini, S., Catena, R., Gansmuller, A., Kotaja, N., Parvinen, M., Sassone-Corsi, P. and Davidson, I. (2005). Polar nuclear localization of H1T2, a histone H1 variant, required for spermatid elongation and DNA condensation during spermiogenesis. *Proc. Natl. Acad. Sci. USA* **102**, 2808-2813.
Matzuk, M. M. and Lamb, D. J. (2002). Genetic dissection of mammalian fertility pathways. *Nat. Cell Biol.* **4 Suppl.**, s41-s49.
Meistrich, M. L. (1993). Nuclear morphogenesis during spermiogenesis. In *Molecular Biology of the Male Reproductive System* (ed. D. de Kretser), pp. 67-97. New York: Academic Press.
Meistrich, M. L., Trostle-Weige, P. K. and Russell, L. D. (1990). Abnormal manchette development in spermatids of azh/azh mutant mice. *Am. J. Anat.* **188**, 74-86.
Mendoza-Lujambio, I., Burfeind, P., Dixkens, C., Meinhardt, A., Hoyer-Fender, S., Engel, W. and Neesen, J. (2002). The Hook1 gene is non-functional in the abnormal spermatozoon head shape (azh) mutant mouse. *Hum. Mol. Genet.* **11**, 1647-1658.
Mittelstaedt, T. and Schoch, S. (2007). Structure and evolution of RIM-BP genes: identification of a novel family member. *Gene* **403**, 70-79.
Mochida, K., Tres, L. L. and Kierszenbaum, A. L. (1999). Structural and biochemical features of fractionated spermatid manchettes and sperm axonemes of the azh/azh mutant mouse. *Mol. Reprod. Dev.* **52**, 434-444.
Nakai, M., Toshimori, K., Yoshinaga, K., Nasu, T. and Hess, R. A. (1998). Carbendazim-induced abnormal development of the acrosome during early phases of spermiogenesis in the rat testis. *Cell Tissue Res.* **294**, 145-152.
Olson, G. E., Winfrey, V. P., Nagdas, S. K., Hill, K. E. and Burk, R. F. (2005). Selenoprotein P is required for mouse sperm development. *Biol. Reprod.* **73**, 201-211.
Sampson, M. J., Decker, W. K., Beaudet, A. L., Ruitenbeek, W., Armstrong, D., Hicks, M. J. and Craigen, W. J. (2001). Immotile sperm and infertility in mice lacking mitochondrial voltage-dependent anion channel type 3. *J. Biol. Chem.* **276**, 39206-39212.
Sapiro, R., Kostetskii, I., Olds-Clarke, P., Gerton, G. L., Radice, G. L. and Strauss, I. J. (2002). Male infertility, impaired sperm motility, and hydrocephalus in mice deficient in sperm-associated antigen 6. *Mol. Cell. Biol.* **22**, 6298-6305.
Shirohzu, H., Kubota, T., Kumazawa, A., Sado, T., Chijiwa, T., Inagaki, K., Suetake, I., Tajima, S., Wakui, K., Miki, Y. et al. (2002). Three novel DNMT3B mutations in Japanese patients with ICF syndrome. *Am. J. Med. Genet.* **112**, 31-37.
Tanaka, H., Iguchi, N., Toyama, Y., Kitamura, K., Takahashi, T., Kaseda, K., Maekawa, M. and Nishimune, Y. (2004). Mice deficient in the axonemal protein Tektin-t exhibit male infertility and immotile-cilium syndrome due to impaired inner arm dynein function. *Mol. Cell. Biol.* **24**, 7958-7964.
Tanaka, H., Iguchi, N., Isotani, A., Kitamura, K., Toyama, Y., Matsuoka, Y., Onishi, M., Masai, K., Maekawa, M., Toshimori, K. et al. (2005). HANP1/H1T2, a novel histone H1-like protein involved in nuclear formation and sperm fertility. *Mol. Cell. Biol.* **25**, 7107-7119.
Toshimori, K. and Ito, C. (2003). Formation and organization of the mammalian sperm head. *Arch. Histol. Cytol.* **66**, 383-396.
Toyama, Y., Kazama, T., Fuse, H. and Katayama, T. (1995). A case of decapitated spermatozoa in an infertile man. *Andrologia* **27**, 165-170.
Toyama, Y., Iwamoto, T., Yajima, M., Baba, K. and Yuasa, S. (2000). Decapitated and decaudated spermatozoa in man, and pathogenesis based on the ultrastructure. *Int. J. Androl.* **23**, 109-115.
Wang, Y., Sugita, S. and Sudhof, T. C. (2000). The RIM/NIM family of neuronal C2 domain proteins. Interactions with Rab3 and a new class of Src homology 3 domain proteins. *J. Biol. Chem.* **275**, 20033-20044.
Xie, Z. H., Huang, Y. N., Chen, Z. X., Riggs, A. D., Ding, J. P., Gowher, H., Jeltsch, A., Sasaki, H., Hata, K. and Xu, G. L. (2006). Mutations in DNA methyltransferase DNMT3B in ICF syndrome affect its regulation by DNMT3L. *Hum. Mol. Genet.* **15**, 1375-1385.
Yang, W. X., Jefferson, H. and Sperry, A. O. (2006). The molecular motor KIFC1 associates with a complex containing nucleoporin NUP62 that is regulated during development and by the small GTPase RAN. *Biol. Reprod.* **74**, 684-690.
Yao, R., Ito, C., Natsume, Y., Sugitani, Y., Yamanaka, H., Kuretake, S., Yanagida, K., Sato, A., Toshimori, K. and Noda, T. (2002). Lack of acrosome formation in mice lacking a Golgi protein, GOPC. *Proc. Natl. Acad. Sci. USA* **99**, 11211-11216.
Yu, Y. E., Zhang, Y., Unni, E., Shirley, C. R., Deng, J. M., Russell, L. D., Weil, M. M., Behringer, R. R. and Meistrich, M. L. (2000). Abnormal spermatogenesis and reduced fertility in transition nuclear protein 1-deficient mice. *Proc. Natl. Acad. Sci. USA* **97**, 4683-4688.

Table S1. Fertilized oocytes in timed matings

Background	*RIM-BP3* genotype	Fertilized oocytes (%)
129sv×ICR	+/+	92.4 (*n*=10)
	–/–	9.3 (*n*=20)
129sv	+/+	70.6 (*n*=4)
	–/–	2.0 (*n*=11)